Birth of the Hydrated Electron via Charge-Transfer-to-Solvent Excitation of Aqueous Iodide

Kevin Carter-Fenk,[1,2,3*] Britta A. Johnson,[1] John M. Herbert,[3†] Gregory K. Schenter,[1] and Christopher J. Mundy[1,4‡]
[1] *Physical Science Division, Pacific Northwest National Laboratory, Richland, Washington 99352, USA*
[2] *Department of Chemistry, University of California, Berkeley, California 94720, USA*
[3] *Department of Chemistry and Biochemistry, The Ohio State University, Columbus, Ohio 43210, USA*
[4] *Department of Chemical Engineering, University of Washington, Seattle, Washington 98195, USA*
(Dated: March 17, 2023)

Abstract

A primary means to generate hydrated electrons in laboratory experiments is excitation to the charge-transfer-to-solvent (CTTS) state of a solute such as $I^-(aq)$, but this initial step in the genesis of $e^-(aq)$ has never been simulated directly using *ab initio* molecular dynamics. We report the first such simulations, combining ground- and excited-state simulations of $I^-(aq)$ with a detailed analysis of fluctuations in the Coulomb potential experienced by the nascent solvated electron. What emerges is a two-step picture of the evolution of $e^-(aq)$ starting from the CTTS state: $I^-(aq)+h\nu \rightarrow I^{-*}(aq) \rightarrow I^{\bullet}(aq) + e^-(aq)$. Notably, the equilibrated ground state of $e^-(aq)$ evolves from $I^{-*}(aq)$ without any nonadiabatic transitions, simply as a result of solvent reorganization. The methodology used here should be applicable to other photochemical electron transfer processes in solution, an important class of problems directly relevant to photocatalysis and energy transfer.

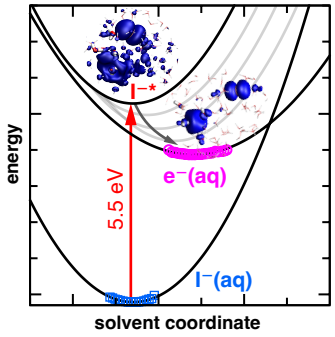

The aqueous or hydrated electron, $e^-(aq)$,[1–4] is a byproduct of ionizing radiation and thus an important reducing agent in radiation chemistry.[1,2] It is also an archetypal quantum-mechanical solute,[4] and thus an important benchmark for solution-phase electron-transfer protocols that has been a target of atomistic simulations for more than three decades.[4–15] Theoretical efforts to understand the properties of $e^-(aq)$ actually predate modern molecular dynamics simulations.[16–18]

Radiochemical origins of $e^-(aq)$ can be probed in the laboratory via pulse radiolysis,[19,20] typically with picosecond time resolution in modern experiments.[20–22] To study the solvation dynamics of $e^-(aq)$ with femtosecond time resolution, a photochemical means to produce $e^-(aq)$ is required.[23,24] A common technique is photodetachment of an aqueous anion such as $I^-(aq)$, $CN^-(aq)$, or $SCN^-(aq)$, accessing its charge-transfer-to solvent (CTTS) bands:[24–30]

$$X^-(aq) + h\nu \rightarrow X^{\bullet}(aq) + e^-(aq) \; .$$

While photodetachment from aqueous halides has been simulated using one-electron pseudopotential models,[31–37] and with many-electron quantum chemistry in $I^-(H_2O)_n$ clusters,[38–40] the present work reports the first *ab initio* simulations of this process in the liquid phase, for X = I.

Previous simulations have established a mechanism whereby a locally-excited (or "trapped") state of $I^{-*}(aq)$, having p → s/d character,[31] rapidly gives way to a "wet" (pre-equilibrated) electron that is not yet fully solvated, culminating in formation of the equilibrated ground state of $e^-(aq)$ after solvent reorganization in the absence of geminate recombination.[31–37] Moving to many-electron *ab initio* simulations can both validate and extend these one-electron results. *e.g.*, to address questions regarding whether the ground state of $e^-(aq)$ genuinely occupies a cavity versus a more delocalized structure,[3] in a manner that is free from concerns regarding the parameterization of one-electron potentials.[41–43] *Ab initio* molecular dynamics simulations of the wet electron have been reported starting from a delocalized state in the conduc-

*carter-fenk@berkeley.edu
†herbert@chemistry.ohio-state.edu
‡chris.mundy@pnnl.gov

tion band,[44,45] but not from the more localized CTTS state. Therefore, the immediate goal of the present work is to investigate the dynamics of threshold photodetachment of I^-(aq) via *ab initio* molecular dynamics. We also present a novel decomposition of the electronic states involved in the charge separation process, which provides a theoretical basis for a mechanism originally put forward by Bradforth and co-workers.[26]

Theoretical description of e^-(aq) presents challenges at the intersection of condensed-phase electronic structure and statistical mechanics. The first challenge in modeling the genesis of e^-(aq) starting from I^-(aq) is to establish a robust simulation protocol. Often in *ab initio* simulations, e^-(aq) is prepared either by adding an electron to neat liquid water, then allowing the system to equilibrate naturally from a delocalized state,[11–13,44–47] or else by creating a cavity in liquid water by means of a proxy ion such as chloride.[48] Although the former approach does afford information regarding the nature of the wet electron[44,45] and of pre-existing trap states in liquid water,[49–51] neither of these protocols directly models the photodetachment mechanism. To develop a consistent picture of the initial and final states, our approach is to allow the system to evolve naturally into the radical–ion pair, $I^{\bullet}$:e^-(aq), starting from the locally excited state, I^{-*}(aq). By developing a single framework to study both the creation and the equilibration of e^-(aq), we may be able to extract statistical-mechanical quantities in addition to spectroscopic properties, eventually encompassing free energies and rates of electron transfer.

The work presented herein adds to the consensus view that the solvated electron resides in the center of an excluded volume or cavity in liquid water.[3] This picture is supported by essentially all recent *ab initio* simulations,[44–48,52–59] as well as numerous earlier simulations based on one-electron pseudopotential models.[4–6,10–15] The present work extends these results via direct simulation of the initial steps in cavity formation starting from I^{-*}(aq) and connecting three different protocols within the framework of density functional theory (DFT). Specifically, we employ (*i*) DFT within the generalized gradient approximation (GGA), in order to generate ensembles of ground-state I^-(aq); (*ii*) hybrid functionals within the restricted open shell Kohn-Sham (ROKS) formalism,[60,61] in order to generate the S_1 state I^{-*}(aq); and (*iii*) ground-state, unrestricted DFT using hybrid functionals, as a means to describe the solvated electron in the presence of $I^{\bullet}$(aq). A hallmark of this study is a demonstration that the S_1 state is accessible by vertical excitation of equilibrated I^-(aq), initially forming a "frustrated Rydberg state",[62] I^{-*}(aq), which initiates cavity formation as it spontaneously evolves into $I^{\bullet}$(aq) + e^-(aq). Connecting these distinct events within an *ab initio* simulation framework affords a Marcus-like picture of the solution-phase electron transfer process, directly from the simulation data.

We began by simulating the ground state of $I^-(H_2O)_{96}$ under periodic boundary conditions with the BLYP+D2 functional.[63–65] Structures generated in these simulations were used to initialize subsequent ROKS simulations of the S_1 state. ROKS is good approach for modeling CT excited states, which are typically well described by a single pair of orbitals. Despite the CT nature of the initial excited state and the favorable accuracy of the ROKS method ($\sim$ 0.2 eV for valence excited states, with only a mild dependence on the choice of functional),[66] we found that the details of the band structure of water were critically important to the subsequent CTTS dynamics. This places some constraints on the choice of functional, as an accurate band gap is a prerequisite for modeling the appropriate CTTS state. We found that ROKS simulations based on BLYP+D2 resulted in S_1 dynamics that sampled a plethora of continuum states in which the electron is delocalized throughout the simulation cell.

The CTTS state of interest ought to lie between the valence and conduction bands,[24] but GGA functionals such as BLYP+D2 dramatically underestimate the band gap.[67–69] This causes continuum states from the conduction band to dip below the CTTS state of I^-(aq). Since we are targeting only the lowest-energy singlet with our ROKS simulations, and the energies of the continuum orbitals of liquid water are artificially low when using BLYP+D2, the S_1 state generated in this way does not afford a hydrated electron. We suggest that this problem originates in underestimation of the band gap by GGAs rather than self-interaction error *per se*, because GGA functionals do predict a bound singly-occupied molecular orbital (SOMO) for e^-(aq), for a variety of different water structures.[56] (Self-interaction error does mean that Kohn-Sham eigenvalues should not be taken seriously as ionization energies unless steps are taken to address this error.[70]) Instead, it would appear that the appropriate CTTS state is simply not found, because states in the conduction band are artificially low in energy.

We ameliorate this band-gap problem by augmenting the PBE functional[71] with 40% exact exchange along with rVV10 nonlocal correlation.[72] (The latter is a revised version of the original VV10 functional.[73]) This composite functional, which we call PBEh(40)-rVV10, predicts an accurate band gap for neat liquid water.[74–76] In the present context, it affords an S_1 state with proper CTTS character, namely, a mid-gap excited state featuring significant charge separation, which rapidly localizes to form e^-(aq) as discussed below.

Now that the CTTS state of I^-(aq) can be generated reliably, we next consider its dynamics. We initiate the excited-state dynamics using ROKS/PBEh(40)-rVV10 atop a randomly-selected nuclear configuration from the ground-state BLYP+D2 trajectory of I^-(aq). Although the electronic band structure obtained from BLYP+D2 is clearly incorrect, our hypothesis is that this functional nevertheless affords a good ground-state hydration structure, which is supported by previous comparisons to experiment.[77–79] To verify that the CTTS excitation generated with ROKS is reproducible, we used several different frames from the ground-state I^-(aq) tra-

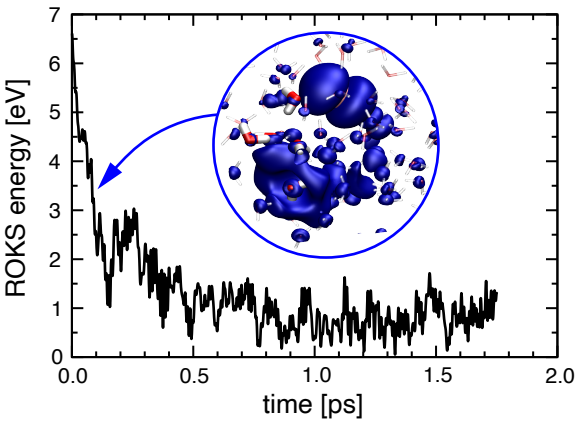

Figure 1: Relaxation of e^-(aq) from the initially excited CTTS state, illustrating fluctuations in the ROKS energy. The frustrated Rydberg state is illustrated at $t = 0.1$ ps following excitation at $t = 0$. The water molecules that eventually coordinate to e^-(aq) are shown using a larger tubular representation.

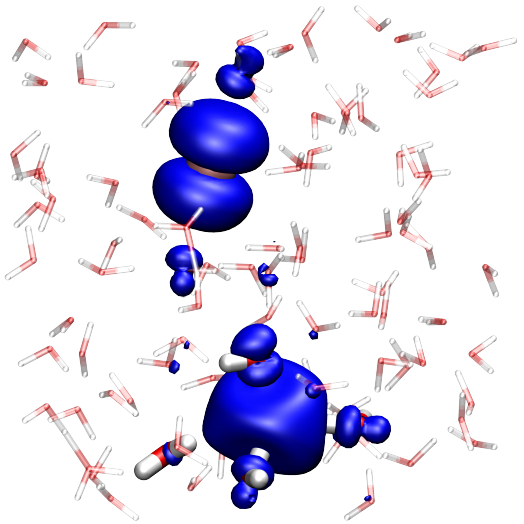

Figure 2: Spin density of I•(aq) and e^-(aq) after electron detachment and localization. At the bottom, the water molecules directly coordinated to e^-(aq) are shown using a larger tubular representation.

jectory to initialize the subsequent ROKS simulation. This revealed that the position of the initially excited electron is highly variable, and different starting configurations along the ground-state trajectory eject the electron to very different positions within the simulation cell. These microstate-dependent fluctuations are illustrated using transition dipole moments obtained from time-dependent (TD-)DFT calculations of the initial CTTS state, as shown in Fig. S2. This is consistent with an electron that is initially "trap-seeking",[3] meaning that inherent (and fluxional) voids in the structure of liquid water[80,81] manifest as variability in the location of the lowest-energy CTTS excitation.

In what follows, we consider the relaxation of a ROKS trajectory in the CTTS state, starting from one particular frame (Fig. 1). Once the frustrated Rydberg state I^{-*}(aq) is formed, the timescale for localization of e^-(aq) is only ~ 250 fs, corresponding to the steep drop in the energy of the S_1 state that is depicted in Fig. 1, and culminating in the solvent-separated ion–radical complex that is depicted in Fig. 2. This suggests a picture in which an initially trap-seeking electron localizes into a pre-existing solvent void,[50] then rapidly stabilizes via anionic solvation. (Electron–water hydrogen bonds[2,12,56] are evident in Fig. 2.) The electron thus transitions from trap-seeking to trap-digging, on what has independently been estimated to be a ~ 250 fs timescale,[3,45] during which time the water molecules reorient to accommodate e^-(aq). Following this rapid initial stabilization, the potential energy continues to decrease (albeit more slowly), until the energy of the CTTS state lies about 0.7 eV above the energy of the I•:e^-(aq) ground state. These timescales are roughly consistent with early-time relaxation dynamics predicted in *ab initio* simulations of electron injection into neat liquid water.[44,45]

We now return to the ground state by removing the constraints of ROKS and re-optimizing the wave function using spin-polarized (unrestricted) orbitals atop a solvent configuration that was generated from 250 fs of ROKS dynamics. In the absence of geminate recombination (a pathway that is not considered in this work), the ground state of e^-(aq) remains localized in the SOMO and separated from I•(aq), from which it gradually diffuses apart as evident from the center-to-center distance that is plotted as a function of time in Fig. S3. At this point, the structural properties of e^-(aq) resemble those of a strongly hydrated anion, whose electron–oxygen radial distribution function (RDF) is plotted in Fig. 3a based on 14 ps of simulation data. We confirm the localization of the SOMO by inspecting centroids of maximally-localized Wannier functions.[82] The second moment of the SOMO's Wannier function is centered around 1.75 Å (Fig. 3b), which is consistent with an excluded volume extending to $r \approx 2$ Å in $g(r)$. An excluded volume of the same size is observed in other simulations performed using the same functional,[45] and in cavity-forming pseudopotential models.[10,12]

Note that the cavity radius suggested by the RDF ($\approx$ 2 Å) is smaller than the radius of gyration ($r_g = 2.45$ Å) that is inferred from the experimental absorption spectrum of e^-(aq).[3,83] Since the Wannier functions are obtained from a localization procedure, we also computed r_g as the second moment of the canonical SOMO computed using an atom-centered Gaussian basis set. These calculations use clusters extracted from the periodic trajectory, containing an average of 157 water molecules plus a larger number of point charges as described in the Computational Details. The result, $\langle r_g \rangle = 2.3 \pm 0.6$ Å, implies that r_g is indeed larger than the radius of the cavity, consistent with a particle-in-a-box model having a finite

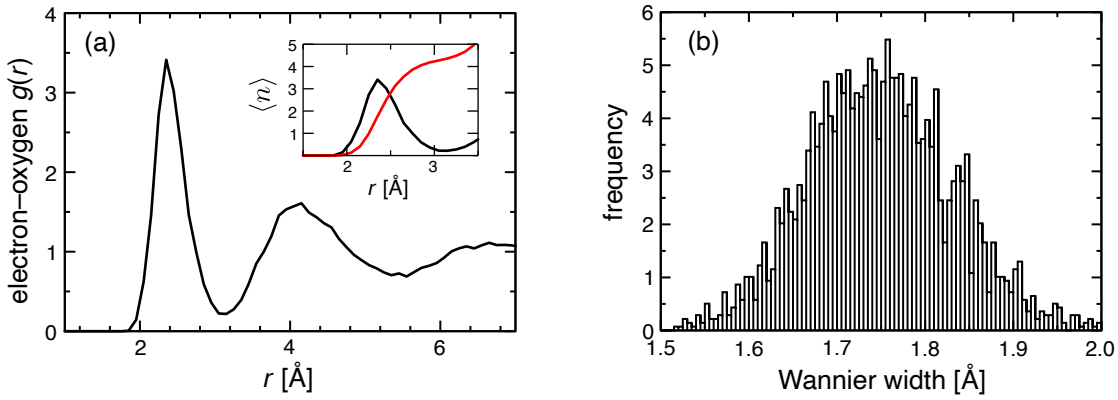

Figure 3: Structural properties of e^-(aq) in equilibrated simulations of I•:e^-(aq), based on 14 ps of simulation data. (a) Electron–oxygen radial distribution function, $g(r)$. The inset plots $g(r)$ (in black) along with the integrated coordination number $\langle n \rangle$ that is obtained from it (in red). (b) Probability distribution for the width (second moment) of the maximally-localized Wannier function corresponding to the SOMO of e^-(aq), computed using spin-polarized orbitals.

well depth.[14] (This observation is also consistent with the fact that the unpaired spin density penetrates into the second solvation shell.[12,14,52]) To make contact with the maximally-localized Wannier functions, which are periodic analogues of Boys-localized MOs,[82] we applied a Boys localization algorithm[84] to the cluster calculations. This reduces the radius of gyration of the orbital that best represents the unpaired electron, from $\langle r_g \rangle = 2.3$ Å (canonical) to $\langle r_g \rangle = 1.5$ Å (Boys-localized), thus explaining the smaller width that is suggested in Fig. 3b based on Wannier functions.

Localization of the CTTS state to form e^-(aq) is associated with significant stabilization of the ROKS potential energy (Fig. 1), driven by reorientation of nearby water molecules in an effort to adapt to a new charge distribution and to form new hydrogen bonds. The electron–oxygen RDF in Fig. 3a shows that the first hydration shell of e^-(aq) extends to 3.1 Å and the integrated $g(r)$ in the inset implies that 4–5 water molecules coordinate to e^-(aq). This is consistent with other *ab initio* simulations of the equilibrated hydrated electron, using the same functional.[46]

Values of r_g obtained in various simulations of e^-(aq) correlate very well with the ground-state excitation energy of the equilibrated species,[6,85] with a r_g^{-2} dependence for the excitation energy that is consistent with a spherical particle-in-a-box potential.[85] TDDFT calculations along the equilibrated I•:e^-(aq) trajectory afford an average excitation energy of 1.91 ± 0.76 eV, computed using a long-range corrected (LRC) functional[86–88] with an "optimally tuned" range-separation parameter,[54,88] as described in the Computational Details. Although this excitation energy is slightly larger than the experimental absorption maximum of 1.7 eV,[2,89] it is consistent with a radius of gyration of $r_g = 2.3$ Å.[85] Remaining discrepancies are well within the intrinsic accuracy of TDDFT.[90]

The *ab initio* picture of the photodetachment process that we have described so far is entirely consistent with the results from one-electron pseudopotential simulations,[31–37] but our *ab initio* protocol offers the intriguing prospect of studying the hydration structure of the iodine radical that is left behind. Incremental iodine–oxygen RDFs for I•:e^- (Fig. 4), which indicate the position of successive neighboring oxygen atoms around the iodine radical in the equilibrated ion–radical ground state, suggest of a highly asymmetric solvation structure in which the closest hydrating water molecule is much closer to I• than any of the others. This nearest-neighbor water molecule is primarily responsible for the first peak in the full iodine–oxygen RDF, in agreement with DFT simulations of I•(aq).[91] In contrast, one-electron pseudopotential models, which describe the intermolecular

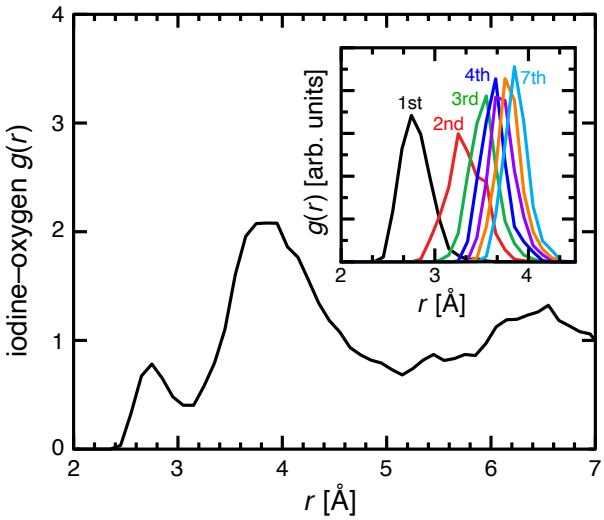

Figure 4: Iodine–oxygen RDF $g(r)$ for the equilibrated ground state of I•:e^-(aq). The inset decomposes $g(r)$ into incremental contributions arising from the nearest oxygen atom (labeled "1st"), second-nearest oxygen atom ("2nd"), etc. These incremental distributions are not normalized.

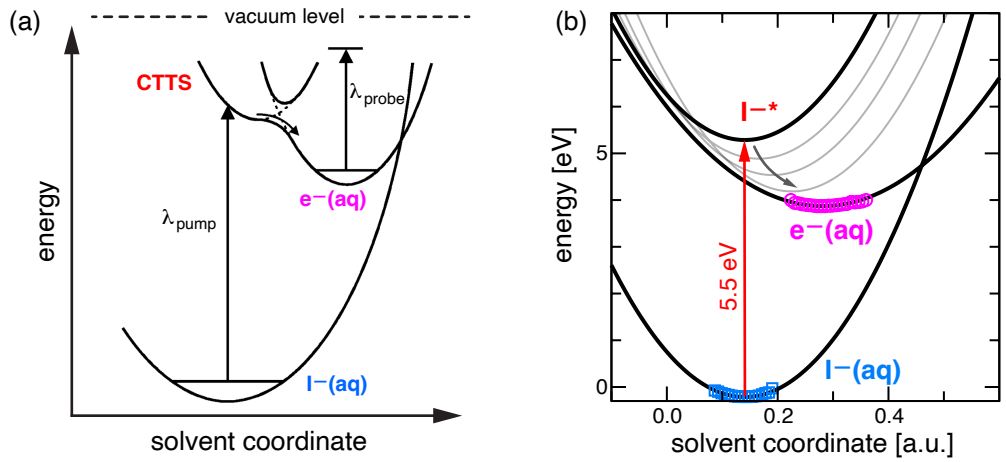

Figure 5: Diabatic models for the emergence of e^-(aq) following CTTS excitation of I^-(aq). (a) The model proposed by Bradforth and workers based on experimental work.[26] (b) Fitted potential energy surfaces obtained from *ab initio* simulations. In (b), the energies obtained from ground-state I^-(aq) trajectories are shown as blue squares and those for equilibrated e^-(aq) are shown as magenta circles. Each set of energies was fit to a Gaussian (black curves). The reaction coordinate along the horizontal axis is a collective solvent coordinate corresponding to the electrostatic potential generated by the water molecules and evaluated at the coordinates of I^- or at the centroid of the SOMO of e^-(aq). The uppermost surface is the CTTS state, which is initially excited at 5.5 eV above the I^-(aq) ground state. Gray parabolas provide a schematic view of solvent relaxation and energetic stabilization of the short-lived CTTS state. Panel (a) is adapted with permission from Kloepfer *et al.*, *J. Chem. Phys.* **2000**, *113*, 6288–6307. Copyright 2000 American institute of Physics.

forces entirely via classical force fields, produce a symmetric solvation environment for I•(aq).[62,91] (It may be possible to describe the asymmetry using polarizable force fields, as in the case of I^-,[92] but this has not been considered in previous one-electron simulations of the photodetachment mechanism.) The good agreement between the iodine–water structural parameters that we obtain for the ion–radical pair I•:e^-, as compared to those obtained for I•(aq) in the absence of a solvated electron,[77,91] suggests that the structure of I•(aq) is not significantly perturbed by the presence of e^-(aq). The ability to describe this asymmetric hydration structure gives *ab initio* simulations a clear advantage over one-electron models for future consideration of geminate recombination pathways that are likely to be strongly influenced by the hydration structure around the radical.

Beyond the molecular picture of e^-(aq) and I•(aq) that is described above, we have an opportunity to construct a reduced statistical framework that is guided by Marcus theory and informed by the simulation data. Bradforth and coworkers[26] have presented a diabatic view of the evolution of e^-(aq), starting from the CTTS state of I^-(aq), which is shown in Fig. 5a and to which we next make contact, based on *ab initio* simulation data.

To determine the shape of the relevant electronic surfaces, we calculated the electrostatic potential generated by the water molecules at the position of either solute species, I^-(aq) or e^-(aq), along the *ab initio* trajectories. (Details can be found in the Supporting Information.) Configurations are binned according to the solvent's electrostatic potential and the resulting histograms are fit to Gaussian functions.[93,94] The electrostatic potential is a promising reaction coordinate along which to construct local potential energy surfaces, because it can encapsulate rearrangement of a large number of solvent molecules. In Fig. 5b, we present the fitted potential surfaces along with the raw histogram data, for the I^-(aq) and e^-(aq) states, and we suggest the relaxation process from the CTTS state to the equilibrated e^-(aq) state.

As the solvent is allowed to reorganize around the I^{-*} intermediate, the CTTS state is stabilized and this appears as a decrease in energy of the CTTS state, as observed in the simulation data (Fig. 1) and shown schematically in Fig. 5b. Solvent relaxation brings the CTTS state into coalescence with the equilibrated ground state of the ion–radical pair. While our simulations exhibit several instances of near-degeneracy between ROKS and e^-(aq), we simply switch to the ground-state potential at these points rather than computing nonadiabatic couplings, which is consistent with the idea that the CTTS $\rightarrow$ e^-(aq) transition can be achieved adiabatically via solvation dynamics.

The picture that emerges from the simulations is therefore substantially similar to that inferred by Bradforth and co-workers,[26] including the strictly adiabatic transition from the CTTS state to e^-(aq). Indeed, a key finding from our simulations is that there is no surface crossing from the CTTS state to e^-(aq), but instead the solvent simply reorganizes to accommodate e^-(aq). Solvent relaxation results in an additional stabilization of $\sim$ 1.5 eV, following the $\sim$ 250 fs localization process that is documented in Fig. 1, which is consistent with

experimentally measured Stokes shifts[95] and with results from one-electron pseudopotential simulations.[34,35] This is also direct evidence of trap-digging behavior, consistent with the interpretation in Ref. 3 that the delocalized wet electron is trap-seeking for its first $\sim$ 250 fs before transitioning to trap-digging behavior at later times. The emergence of a 250-fs timescale is consistent with ultrafast spectroscopy[25–27] and with one-electron simulation results.[35–37]

The following picture emerges to describe the "birth" of e^-(aq) from the CTTS state. Vertical excitation into the CTTS state is microstate-dependent (trap-seeking), due to the nonuniform nature of the solvent fluctuations, but this frustrated Rydberg state is short-lived. It localizes to form e^-(aq) in $\sim$ 250 fs and fully equilibrates to the ground state of I$^\bullet$:e^-(aq) within $\sim$ 1 ps, via solvent relaxation or trap-digging behavior. This species remains within the Marcus inverted region (Fig. 5b), consistent with the picture put forward by Bradforth and co-workers (Fig. 5a).[26]

Thus, we have presented a fully *ab initio* protocol for generating e^-(aq) from the ground state of an aqueous anion. The picture that emerges naturally from the simulations is roughly consistent with the known vertical excitation energies of I^-(aq) and e^-(aq), with structural properties of e^-(aq) including coordination number and radius of gyration, and also with the relative energies of the I^-(aq) and I$^\bullet$:e^-(aq) ground states. A Marcus-like picture can be inferred from fluctuations in the solvent's electrostatic potential, consistent with the reaction path used to understand the experimental photodetachment dynamics of I^-(aq),[26] yet a refined understanding of the locally excited I^{-*} intermediate emerges from the simulations. The initially delocalized electron is trap-seeking following vertical excitation but rapidly transitions to a trap-digging species that drives significant solvent relaxation, without any nonadiabatic surface crossings. This suggests that the photo-induced electron transfer rate from halide to solvent is limited by solvent reorganization. Our approach may provide a useful cornerstone upon which *ab initio* simulations of solution-phase electron-transfer parameters[76,96] can be performed, in order to described photo-induced electron transfer in solution.

Computational Methods

Ab initio molecular dynamics simulations on $I^-(H_2O)_{96}$, in a $(14.4\ \text{Å})^3$ unit cell, were performed using CP2K v. 9.1.[97] These simulations used either the BLYP+D2 functional[63–65] or the PBEh(40)-rVV10 functional,[46] with the DZVP-MOLOPT basis set.[98] (Following Ref. 46, we set the parameter $b = 5.3$ in rVV10.) Temperature was maintained at $T = 298$ K using canonical sampling with velocity rescaling.[99] The procedure used to generate Fig. 5 is described in the Supporting Information.

The ground-state wave function of I$^\bullet$:e^- was found to have triplet multiplicity, which may be a consequence of our neglect of spin-orbit effects, as the singlet does not yield a solvent-separated ion–radical pair, but the triplet has been found to be a reasonable proxy for modeling CTTS dynamics.[62] Spin-orbit corrections have been introduced for ROKS simulations only very recently,[100] and these effects are neglected here. Experimentally, the spin-orbit coupling splits the CTTS spectrum of I^-(aq) into $^2P_{3/2}$ and $^2P_{1/2}$ bands centered at 5.5 eV and 6.44 eV, respectively.[24] A spin-orbit-free excitation energy can be estimated from these experimental values as $[E(^2P_{1/2}) + 2E(^2P_{3/2})]/3 = 5.8$ eV,[101,102] which is roughly in line with our ROKS excitation energies.

Calculations in atom-centered basis sets were performed using a quantum mechanics/molecular mechanics (QM/MM) protocol used previously for e^-(aq),[15,54,56] in which water molecules within 8.5 Å of the iodine atom (along with iodine itself) were included in the QM region, for an average of 157 water molecules per snapshot. This requires periodic replication of the unit cell and the periodic images of iodine were omitted. Additional water molecules were included as MM point charges, out to a radius of 30 Å. These calculations were performed with Q-Chem v. 6.0,[103] using the PBEh(40)-rVV10 functional and the minimally-augmented def2-ma-SVP basis set[104] for the ground-state r_g calculations. For TDDFT calculations, we used LRC-ωPBEh(40)-rVV10/def2-ma-SVP with a tuned range-separation parameter, $\omega = 0.24\ \text{bohr}^{-1}$. The value of ω was determined using the global density-dependent tuning procedure,[105–107] as in previous work on the CTTS state of I^-(aq).[76] This approach is a convenient alternative to "optimal tuning" based on the ionization energy condition.[88]

Supporting Information

Details of the procedure used to analyze fluctuations in the Coulomb potential along with additional analysis of the trajectories.

Notes

The authors declare the following competing financial interest(s): J.M.H. serves on the board of directors of Q-Chem Inc.

Acknowledgements

K.C.-F. acknowledges support from the U.S. Department of Energy (DOE) Office of Science, Office of Workforce Development for Teachers and Scientists, Office of Science Graduate Student Research (SCGSR) program. The SCGSR program is administered by the Oak Ridge Institute for Science and Education (ORISE) for the DOE. ORISE is managed by ORAU under contract

number DE-SC0014664. J.M.H. acknowledges support from the National Science Foundation (grant no. CHE-1955282). B.A.J, C.J.M., and G.K.S. are supported by the DOE Office of Science, Office of Basic Energy Sciences, Division of Chemical Sciences, Geosciences, and Biosciences. All opinions expressed in this paper are the author's and do not necessarily reflect the policies and views of DOE, ORAU, or ORISE. Calculations were performed on both Pacific Northwest National Laboratory's Institutional Computing resource, the National Energy Research Scientific Computing Center (NERSC), and the Ohio Supercomputer Center.[108] NERSC is a U.S. Department of Energy Office of Science User Facility located at Lawrence Berkeley National Laboratory, operated under Contract No. DE-AC02-05CH11231.

References

[1] Alizadeh, E.; Sanche, L. Precursors of solvated electrons in radiobiological physics and chemistry. *Chem. Rev.* **2012,** *112,* 5578–5602.

[2] Herbert, J. M.; Coons, M. P. The hydrated electron. *Annu. Rev. Phys. Chem.* **2017,** *68,* 447–472.

[3] Herbert, J. M. Structure of the aqueous electron. *Phys. Chem. Chem. Phys.* **2019,** *21,* 20538–20565.

[4] Turi, L.; Rossky, P. J. Theoretical studies of spectroscopy and dynamics of hydrated electrons. *Chem. Rev.* **2012,** *112,* 5641–5674.

[5] Rossky, P. J.; Schnitker, J.; Kuharski, R. A. Quantum simulation of aqueous systems. *J. Stat. Phys.* **1986,** *43,* 949–965.

[6] Rossky, P. J.; Schnitker, J. The hydrated electron: Quantum simulation of structure, spectroscopy, and dynamics. *J. Phys. Chem.* **1988,** *92,* 4277–4285.

[7] Coker, D. F.; Berne, B. J.; Thirumalai, D. Path integral Monte Carlo studies of the behavior of excess electrons in simple fluids. *J. Chem. Phys.* **1987,** *86,* 5689–5702.

[8] Wallqvist, A.; Thirumalai, D.; Berne, B. J. Path integral Monte Carlo study of the hydrated electron. *J. Chem. Phys.* **1987,** *86,* 6404–6418.

[9] Coker, D. F.; Berne, B. J. Quantum calculations on excess electrons in disordered media. In *Excess Electrons in Dielectric Media*; Ferradini, C.; Jay-Gerin, J.-P., Eds.; CRC Press: Boca Raton, FL, 1991; Chapter 7, pages 211–258.

[10] Turi, L.; Borgis, D. Analytical investigations of an electron–water molecule pseudopotential. II. Development of a new pair potential and molecular dynamics simulations. *J. Chem. Phys.* **2002,** *117,* 6186–6195.

[11] Jacobson, L. D.; Herbert, J. M. Polarization-bound quasi-continuum states are responsible for the 'blue tail' in the optical absorption spectrum of the aqueous electron. *J. Am. Chem. Soc.* **2010,** *132,* 10000–10002.

[12] Jacobson, L. D.; Herbert, J. M. A one-electron model for the aqueous electron that includes many-body electron-water polarization: Bulk equilibrium structure, vertical electron binding energy, and optical absorption spectrum. *J. Chem. Phys.* **2010,** *133,* 154506.

[13] Coons, M. P.; You, Z.-Q.; Herbert, J. M. The hydrated electron at the surface of neat liquid water appears to be indistinguishable from the bulk species. *J. Am. Chem. Soc.* **2016,** *138,* 10879–10886.

[14] Herbert, J. M.; Jacobson, L. D. Nature's most squishy ion: The important role of solvent polarization in the description of the hydrated electron. *Int. Rev. Phys. Chem.* **2011,** *30,* 1–48.

[15] Herbert, J. M.; Jacobson, L. D. Structure of the aqueous electron: Assessment of one-electron pseudopotential models in comparison to experimental data and time-dependent density functional theory. *J. Phys. Chem. A* **2011,** *115,* 14470–14483.

[16] Jortner, J.; Rice, S. A. Theoretical studies of solvated electrons. In *Solvated Electron*, Vol. 50; Gould, R. F., Ed.; American Chemical Society Publications: Washington, D.C., 1965; Chapter 2, pages 7–26.

[17] Copeland, D. A.; Kestner, N. R.; Jortner, J. Excess electrons in polar solvents. *J. Chem. Phys.* **1970,** *53,* 1189–1216.

[18] Feng, D.-F.; Kevan, L. Theoretical models for solvated electrons. *Chem. Rev.* **1980,** *80,* 1–20.

[19] Boag, J. W. Pulse radiolysis: A historical account of the discovery of the optical absorption spectrum of the hydrated electron. In *Early Developments in Radiation Chemistry*; Kroh, J., Ed.; Royal Society of Chemistry: Cambridge, UK, 1989; Chapter 2, pages 7–20.

[20] Muroya, Y.; Lin, M.; Han, Z.; Kumagai, Y.; Sakumi, A.; Ueda, T.; Katsumura, Y. Ultra-fast pulse radiolysis: A review of the recent system progress and its application to study on initial yields and solvation processes of solvated electrons in various kinds of alcohols. *Radiat. Phys. Chem.* **2008,** *77,* 1176–1182.

[21] Muroya, Y.; Watanabe, T.; Wu, G.; Li, X.; Kobayashi, T.; Sugahara, J.; Ueda, T.; Yoshii, K.; Uesaka, M.; Katsumura, Y. Design and development of a sub-picosecond pulse radiolysis system. *Radiat. Phys. Chem.* **2001,** *60,* 307–312.

[22] Ma, J.; Schmidhammer, U.; Mostafavi, M. Direct evidence for transient pair formation between a solvated electron and H_3O^+ observed by picosecond pulse radiolysis. *J. Phys. Chem. Lett.* **2014,** *5,* 2219–2223.

[23] Signorell, R.; Winter, B. Photoionization of the aqueous phase: Clusters, droplets and liquid jets. *Phys. Chem. Chem. Phys.* **2022,** *24,* 13438–13460.

[24] Chen, X.; Bradforth, S. E. The ultrafast dynamics of photodetachment. *Annu. Rev. Phys. Chem.* **2008,** *59,* 203–231.

[25] Kloepfer, J. A.; Vilchiz, V. H.; Lenchenkov, V. A.; Bradforth, S. E. Femtosecond dynamics of photodetachment of the iodide anion in solution: Resonant excitation into the charge-transfer-to-solvent state. *Chem. Phys. Lett.* **1998,** *298,* 120–128.

[26] Kloepfer, J. A.; Vilchiz, V. H.; Lenchenkov, V. A.; Germaine, A. C.; Bradforth, S. E. The ejection distribution of solvated electrons generated by the one-photon photodetachment of aqueous I^- and two-photon ionization of the solvent. *J. Chem. Phys.* **2000,** *113,* 6288–6307.

[27] Vilchiz, V. H.; Kloepfer, J. A.; Germaine, A. C.; Lenchenkov, V. A.; Bradforth, S. E. Map for the relaxation dynamics of hot photoelectrons injected into liquid water via anion threshold photodetachment and above threshold solvent ionization. *J. Phys. Chem.* **2001,** *105,* 1711–1723.

[28] Kloepfer, J. A.; Vilchiz, V. H.; Lenchenkov, V. A.; Chen, X.; Bradforth, S. E. Time-resolved scavenging and recombination dynamics from I:e^- caged pairs. *J. Chem.*

Phys. **2002,** *117,* 766–778.
[29] Rizzuto, A. M.; Irgen-Gioro, S.; Eftekhari-Bafrooei, A.; Saykally, R. J. Broadband deep UV spectra of interfacial aqueous iodide. *J. Phys. Chem. Lett.* **2016,** *7,* 3882–3885.
[30] Bhattacharyya, D.; Mizuno, H.; Rizzuto, A. M.; Zhang, Y.; Saykally, R. J.; Bradforth, S. E. New insights into the charge-transfer-to-solvent spectrum of aqueous iodide: Surface versus bulk. *J. Phys. Chem. Lett.* **2020,** *11,* 1656–1661.
[31] Sheu, W.-S.; Rossky, P. J. The electronic dynamics of photoexcited aqueous iodide. *Chem. Phys. Lett.* **1993,** *202,* 186–190.
[32] Sheu, W.-S.; Rossky, P. J. Dynamics of electron photodetachment from an aqueous halide ion. *Chem. Phys. Lett.* **1993,** *213,* 233–238.
[33] Sheu, W.-S.; Rossky, P. J. Charge-transfer-to-solvent spectra of an aqueous halide revisited via computer simulation. *J. Am. Chem. Soc.* **1993,** *115,* 7729–7739.
[34] Sheu, W.-S.; Rossky, P. J. Electronic and solvent relaxation dynamics of a photoexcited aqueous halide. *J. Phys. Chem.* **1996,** *100,* 1295–1302.
[35] Staib, A.; Borgis, D. Reaction pathways in the photodetachment of an electron from aqueous chloride: A quantum molecular dynamics study. *J. Chem. Phys.* **1996,** *104,* 9027–9039.
[36] Borgis, D.; Staib, A. Excited states of a hydrated electron and aqueous chloride by computer simulation. *Chem. Phys. Lett.* **1994,** *230,* 405–413.
[37] Borgis, D.; Staib, A. Quantum adiabatic umbrella sampling: The excited state free energy surface of an electron-atom pair in solution. *J. Chem. Phys.* **1996,** *104,* 4776–4783.
[38] Chen, H. Y.; Sheu, W.-S. Precursors of the charge-transfer-to-solvent states in $I^-(H_2O)_n$ clusters. *J. Am. Chem. Soc.* **2000,** *122,* 7534–7542.
[39] Elola, M. D.; Laria, D. Solvation dynamics following electron photodetachment from I^- in aqueous clusters. *J. Chem. Phys.* **2002,** *117,* 2238–2245.
[40] Timerghazin, O. K.; Peslherbe, G. H. Further insight into the relaxation dynamics of photoexcited $I^-(H_2O)_n$ clusters. *J. Am. Chem. Soc.* **2003,** *125,* 9904–9905.
[41] Turi, L.; Madarász, A. Comment on "Does the hydrated electron occupy a cavity?". *Science* **2011,** *331,* 1387.
[42] Jacobson, L. D.; Herbert, J. M. Comment on "Does the hydrated electron occupy a cavity?". *Science* **2011,** *331,* 1387.
[43] Glover, W. J.; Schwartz, B. J. Short-range electron correlation stabilizes noncavity solvation of the hydrated electron. *J. Chem. Theory Comput.* **2016,** *12,* 5117–5131.
[44] Savolainen, J.; Uhlig, F.; Ahmed, S.; Hamm, P.; Jungwirth, P. Direct observation of the collapse of the delocalized excess electron in water. *Nat. Chem.* **2014,** *6,* 697–701.
[45] Pizzochero, M.; Ambrosio, F.; Pasquarello, A. Picture of the wet electron: A localized transient state in liquid water. *Chem. Sci.* **2019,** *10,* 7442–7448.
[46] Ambrosio, F.; Miceli, G.; Pasquarello, A. Electronic levels of excess electrons in liquid water. *J. Phys. Chem. Lett.* **2017,** *8,* 2055–2059.
[47] Lan, J.; Kapil, V.; Gasparotto, P.; Ceriotti, M.; Iannuzzi, M.; Rybkin, V. V. Simulating the ghost: Quantum dynamics of the solvated electron. *Nat. Commun.* **2021,** *12,* 766.
[48] Wilhelm, J.; VandeVondele, J.; Rybkin, V. V. Dynamics of the bulk hydrated electron from many-body wavefunction theory. *Angew. Chem. Int. Ed. Engl.* **2019,** *58,* 3890–3893.
[49] Schnitker, J.; Rossky, P. J.; Kenney-Wallace, G. A. Electron localization in liquid water: A computer simulation study of microscopic trapping sites. *J. Chem. Phys.* **1986,** *85,* 2986–2998.
[50] Bartczak, W. M.; Pernal, K. Potential traps for an excess electron in liquid water. Geometry, energy distributions and lifetime. *Comput. Chem.* **2000,** *24,* 469–482.
[51] Bartczak, W. M.; Pernal, K. Potential traps for an excess electron in liquid water: The trap lifetime distributions. *Res. Chem. Intermed.* **2001,** *27,* 891–900.
[52] Uhlig, F.; Marsalek, O.; Jungwirth, P. Unraveling the complex nature of the hydrated electron. *J. Phys. Chem. Lett.* **2012,** *3,* 3071–3075.
[53] Marsalek, O.; Uhlig, F.; VandeVondele, J.; Jungwirth, P. Structure, dynamics, and reactivity of hydrated electrons by ab initio molecular dynamics. *Acc. Chem. Res.* **2012,** *45,* 23–32.
[54] Uhlig, F.; Herbert, J. M.; Coons, M. P.; Jungwirth, P. Optical spectroscopy of the bulk and interfacial hydrated electron from ab initio calculations. *J. Phys. Chem. A* **2014,** *118,* 7507–7515.
[55] Holden, Z. C.; Rana, B.; Herbert, J. M. Analytic energy gradients for the QM/MM-Ewald method using atomic charges derived from the electrostatic potential: Theory, implementation, and application to *ab initio* molecular dynamics of the aqueous electron. *J. Chem. Phys.* **2019,** *150,* 144115.
[56] Dasgupta, S.; Rana, B.; Herbert, J. M. *Ab initio* investigation of the resonance Raman spectrum of the hydrated electron. *J. Phys. Chem. B* **2019,** *123,* 8074–8084.
[57] Shen, Z.; Peng, S.; Glover, W. J. Flexible boundary layer using exchange for embedding theories. II. QM/MM dynamics of the hydrated electron. *J. Chem. Phys.* **2021,** *155,* 224113.
[58] Lan, J.; Rybkin, V. V.; Pasquarello, A. Temperature dependent properties of the aqueous electron. *Angew. Chem. Int. Ed. Engl.* **2022,** *61,* e202209398.
[59] Li, X.; Jia, X.; Paz, A. S. P.; Cao, Y.; Glover, W. J. Evidence for water antibonding orbital mixing in the hydrated electron from its oxygen 1s x-ray absorption spectrum. *J. Am. Chem. Soc.* **2022,** *144,* 19668–19672.
[60] Frank, I.; Hutter, J.; Marx, D.; Parrinello, M. Molecular dynamics in low-spin excited states. *J. Chem. Phys.* **1998,** *108,* 4060–4069.
[61] Odelius, M.; Laikov, D.; Hutter, J. Excited-state geometries within time-dependent and restricted open-shell density functional theories. *J. Mol. Struct. (Theochem)* **2003,** *630,* 163–175.
[62] Bradforth, S. E.; Jungwirth, P. Excited states of iodide anions in water: A comparison of the electronic structure in clusters and in bulk solution. *J. Phys. Chem.* **2002,** *106,* 1286–1298.
[63] Becke, A. D. Density-functional exchange-energy approximation with correct asymptotic behavior. *Phys. Rev. A* **1988,** *38,* 3098–3100.
[64] Lee, C.; Yang, W.; Parr, R. G. Development of the Colle-Salvetti correlation-energy formula into a functional of the electron density. *Phys. Rev. B* **1988,** *37,* 785–789.
[65] Grimme, S. Semiempirical GGA-type density functional constructed with a long-range dispersion correction. *J. Comput. Chem.* **2006,** *27,* 1787–1799.

[66] Hait, D.; Head-Gordon, M. Orbital optimized density functional theory for electronic excited states. *J. Phys. Chem. Lett.* **2020,** *12,* 4517–4529.

[67] Sham, L. J.; Schlüter, M. Density-functional theory of the energy gap. *Phys. Rev. Lett.* **1983,** *51,* 1888–1891.

[68] Godby, R. W.; Schlüter, M.; Sham, L. J. Accurate exchange-correlation potential for silicon and its discontinuity on addition of an electron. *Phys. Rev. Lett.* **1986,** *56,* 2415–2418.

[69] Sham, L. J.; Schlüter, M. Density-functional theory of the band gap. *Phys. Rev. B* **1985,** *32,* 3883–3889.

[70] Tellez, J. A. V.; Ufondu, P.; Baruah, T.; Yamamoto, Y.; Jackson, K. A.; Zope, R. Importance of self-interaction-error removal in density functional calculations on water cluster anions. *Phys. Chem. Chem. Phys.* **2020,** *22,* 3789–3799.

[71] Perdew, J. P.; Burke, K.; Ernzerhof, M. Generalized gradient approximations made simple. *Phys. Rev. Lett.* **1996,** *77,* 3865–3868.

[72] Sabatini, R.; Gorni, T.; de Gironcoli, S. Nonlocal van der Waals density functional made simple and efficient. *Phys. Rev. B* **2013,** *87,* 041108(R).

[73] Vydrov, O. A.; Van Voorhis, T. Nonlocal van der Waals density functional: The simpler the better. *J. Chem. Phys.* **2010,** *133,* 244103.

[74] Ambrosio, F.; Miceli, G.; Pasquarello, A. Redox levels in aqueous solution: Effect of van der Waals interactions and hybrid functionals. *J. Chem. Phys.* **2015,** *143,* 244508.

[75] Ambrosio, F.; Guo, Z.; Pasquarello, A. Absolute energy levels of liquid water. *J. Phys. Chem. Lett.* **2018,** *9,* 3212–3216.

[76] Carter-Fenk, K.; Mundy, C. J.; Herbert, J. M. Natural charge-transfer analysis: Eliminating spurious charge-transfer states in time-dependent density functional theory via diabatization, with application to projection-based embedding. *J. Chem. Theory Comput.* **2021,** *17,* 4195–4210.

[77] Fulton, J. L.; Schenter, G. K.; Baer, M. D.; Mundy, C. J.; Dang, L. X.; Balasubramanian, M. Probing the hydration structure of polarizable halides: A multiedge XAFS and molecular dynamics study of the iodide anion. *J. Phys. Chem. B* **2010,** *114,* 12926–12937.

[78] Baer, M. D.; Mundy, C. J. Toward an understanding of the specific ion effect using density functional theory. *J. Phys. Chem. Lett.* **2011,** *2,* 1088–1093.

[79] Baer, M. D.; Mundy, C. J. An *ab initio* approach to understanding the specific ion effect. *Faraday Discuss.* **2013,** *160,* 89–101.

[80] Ansari, N.; Laio, A.; Hassanali, A. Spontaneously forming dendritic voids in liquid water can host small polymers. *J. Phys. Chem. Lett.* **2019,** *10,* 5585–5591.

[81] Schönfeldová, T.; Dupertuis, N.; Chen, Y.; Ansari, N.; Poli, E.; Wilkins, D. M.; Hassanali, A.; Roke, S. Charge gradients around dendritic voids cause nanoscale inhomogeneities in liquid water. *J. Phys. Chem. Lett.* **2022,** *13,* 7462–7468.

[82] Berghold, G.; Mundy, C. J.; Romero, A. H.; Hutter, J.; Parrinello, M. General and efficient algorithms for obtaining maximally localized Wannier functions. *Phys. Rev. B* **2000,** *61,* 10040–10048.

[83] Bartels, D. M. Moment analysis of hydrated electron cluster spectra: Surface or internal states? *J. Chem. Phys.* **2001,** *115,* 4404–4405.

[84] Subotnik, J. E.; Shao, Y.; Liang, W.; Head-Gordon, M. An efficient method for calculating maxima of homogeneous functions of orthogonal matrices: Applications to localized occupied orbitals. *J. Chem. Phys.* **2004,** *121,* 9220–9229.

[85] Jacobson, L. D.; Herbert, J. M. Theoretical characterization of four distinct isomer types in hydrated-electron clusters, and proposed assignments for photoelectron spectra of water cluster anions. *J. Am. Chem. Soc.* **2011,** *133,* 19889–19899.

[86] Lange, A. W.; Rohrdanz, M. A.; Herbert, J. M. Charge-transfer excited states in a π-stacked adenine dimer, as predicted using long-range-corrected time-dependent density functional theory. *J. Phys. Chem. B* **2008,** *112,* 6304–6308.

[87] Richard, R. M.; Herbert, J. M. Time-dependent density-functional description of the $^1\mathrm{L}_a$ state in polycyclic aromatic hydrocarbons: Charge-transfer character in disguise? *J. Chem. Theory Comput.* **2011,** *7,* 1296–1306.

[88] Alam, B.; Morrison, A. F.; Herbert, J. M. Charge separation and charge transfer in the low-lying excited states of pentacene. *J. Phys. Chem. C* **2020,** *124,* 24653–24666.

[89] Jou, F.-Y.; Freeman, G. R. Temperature and isotope effects on the shape of the optical absorption spectrum of solvated electrons in water. *J. Phys. Chem.* **1979,** *83,* 2383–2387.

[90] Herbert, J. M. Density functional theory for electronic excited states. In *Theoretical and Computational Photochemistry: Fundamentals, Methods, Applications and Synergy with Experimental Approaches*; García-Iriepa, C.; Marazzi, M., Eds.; Elsevier: 2023; Chapter 3 (in press; preprint available at DOI: 10.48550/arXiv.2204.10135).

[91] Reidelbach, M.; Schneeberger, M.; Zöllner, M. S.; Bai, M.; Kubicek, K.; Kirchberg, H.; Bressler, C.; Thorwart, M.; Herrmann, C. Solvent dynamics of aqueous halides before and after photoionization. (Preprint, DOI: 10.26434/chemrxiv-2022-zkl9j).

[92] Wick, C. D.; Xantheas, S. S. Computational investigation of the first solvation shell structure of interfacial and bulk aqueous chloride and iodide ions. *J. Phys. Chem. B* **2009,** *113,* 4141–4146.

[93] Kuharski, R. A.; Bader, J. S.; Chandler, D.; Sprik, M.; Klein, M. L.; Imprey, R. W. Molecular model for aqueous ferrous–ferric electron transfer. *J. Chem. Phys.* **1988,** *89,* 3248–3257.

[94] Straus, J. B.; Calhoun, A.; Voth, G. A. Calculation of solvent free energies for heterogeneous electron transfer at the water–metal interface: Classical versus quantum behavior. *J. Chem. Phys.* **1995,** *102,* 529–539.

[95] Messina, F.; Bräm, O.; Cannizzo, A.; Chergui, M. Real-time observation of the charge transfer to solvent dynamics. *Nat. Commun.* **2013,** *4,* 1–6.

[96] Roy, S.; Galib, M.; Schenter, G. K.; Mundy, C. J. On the relation between Marcus theory and ultrafast spectroscopy of solvation kinetics. *Chem. Phys. Lett.* **2018,** *692,* 407–415.

[97] Kühne, T. D. *et al.* CP2K: An electronic structure and molecular dynamics software package—Quickstep: Efficient and accurate electronic structure calculations. *J. Chem. Phys.* **2020,** *152,* 194103.

[98] VandeVondele, J.; Hutter, J. Gaussian basis sets for accurate calculations on molecular systems in gas and condensed phases. *J. Chem. Phys.* **2007,** *127,* 114105.

[99] Bussi, G.; Donadio, D.; Parrinello, M. Canonical sampling through velocity rescaling. *J. Chem. Phys.* **2007,**

126, 014101.

[100] Mališ, M.; Vandaele, E.; Luber, S. Spin-orbit couplings for nonadiabatic molecular dynamics at the ΔSCF level. *J. Chem. Theory Comput.* **2022,** *18*, 4082–4094.

[101] Maruani, J.; Kuleff, A. I.; Chong, D. P.; Bonnelle, C. *Ansatz* for the evaluation of the relativistic contributions to core ionization energies in complex molecules involving heavy atoms. *Int. J. Quantum Chem.* **2005,** *104*, 397–410.

[102] Paul, S. K.; Herbert, J. M. Probing interfacial effects on ionization energies: The surprising banality of anion–water hydrogen bonding at the air/water interface. *J. Am. Chem. Soc.* **2021,** *143*, 10189–10202.

[103] Epifanovsky, E. *et al.* Software for the frontiers of quantum chemistry: An overview of developments in the Q-Chem 5 package. *J. Chem. Phys.* **2021,** *155*, 084801.

[104] Gray, M.; Herbert, J. M. Comprehensive basis-set testing of extended symmetry-adapted perturbation theory and assessment of mixed-basis combinations to reduce cost. *J. Chem. Theory Comput.* **2022,** *18*, 2308–2330.

[105] Modrzejewski, M.; Rajchel, Ł.; Chalasinski, G.; Szczesniak, M. M. Density-dependent onset of the long-range exchange: A key to donor–acceptor properties. *J. Phys. Chem. A* **2013,** *117*, 11580–11586.

[106] Lao, K. U.; Herbert, J. M. Atomic orbital implementation of extended symmetry-adapted perturbation theory (XSAPT) and benchmark calculations for large supramolecular complexes. *J. Chem. Theory Comput.* **2018,** *14*, 2955–2978.

[107] Gray, M.; Herbert, J. M. Simplified tuning of long-range corrected density functionals for symmetry-adapted perturbation theory. *J. Chem. Phys.* **2021,** *155*, 034103.

[108] "Ohio Supercomputer Center", http://osc.edu/ark:/19495/f5s1ph73 (accessed 2022-01-08).